Editors' Suggestion

Distinguishing Nonlinear Terahertz Excitation Pathways with Two-Dimensional Spectroscopy

Courtney L. Johnson, Brittany E. Knighton, and Jeremy A. Johnson*
Department of Chemistry and Biochemistry, Brigham Young University, Provo, Utah 84602, USA

(Received 7 November 2018; published 21 February 2019)

High-field terahertz (THz) spectroscopy is enabling the ultrafast study and control of matter in new and exciting ways. However, when intense electromagnetic pulses are used in any kind of pump-probe spectroscopy, several nonlinear excitation pathways can result, leading to scenarios that required the development of multidimensional spectroscopies to illuminate the observed dynamics. Here we demonstrate a clear example where two-dimensional (2D) THz vibrational spectroscopy is needed to distinguish between nonlinear-excitation pathways in $CdWO_4$. We nonlinearly excite a set of Raman-active vibrational modes in $CdWO_4$ with broadband THz pulses, and 2D spectroscopy allows us to determine the dominant excitation pathway. We provide a general framework for 2D THz and multi-THz nonlinear phonon spectroscopy in solid systems, which has important implications in contributing needed clarity to the nascent field of nonlinear phononics.

DOI: 10.1103/PhysRevLett.122.073901

Terahertz (THz) spectroscopy has been growing in prominence and promise over the last 20 years with applications including chemical recognition [1], security and imaging [2], nondestructive testing [3,4], studying nuanced interactions in biological systems [5], extremely high-bandwidth wireless communication, and developing future generation high-speed devices [6]. Recent advances in high-field THz generation [7–15] have introduced nonlinear THz optics and the ability to study nonlinear sample responses with THz excitation, opening up a new realm of experimental avenues to pursue.

Intense THz electric-field pulses have proven useful in observing fascinating effects in a number of materials [16,17]; examples include accelerating electrons to high momentum states [18–21] and perturbing electronic properties of a system to induce an insulator-to-metal transition [22]. THz and multi-THz excitation of vibrational modes to extreme amplitudes has allowed the experimental extraction of the interatomic potential energy surface along certain vibrational coordinates [23,24]. Strong THz radiation enabled the first direct observation of an electromagnon in multiferroic $TbMnO_3$ [25].

Extreme excitation of materials can result in multiple energy-flow pathways, and multidimensional spectroscopy can help disentangle the dynamics, as has been shown with 2D (and higher-order) nuclear magnetic resonance and optical spectroscopies [26,27]. It is clear that many complex sample responses can only be understood and evaluated with multidimensional spectroscopy. However, there are only a handful of examples of 2D spectroscopy involving THz excitation. The Elsaesser group used 2D multi-THz spectroscopy to examine electronic excitations in solids [28,29], the Nelson group used 2D THz spectroscopy to study collective spin waves and coherent rotational motion of gases [30,31], and the Blake group reported 2D THz spectroscopy studies of molecular vibrations in liquids [32,33]. Here, we utilize intense THz electric fields to nonlinearly drive vibrational modes in $CdWO_4$. This work contains an example of 2D-THz phonon spectroscopy in crystalline $CdWO_4$, and as described below, 2D spectroscopy provides the necessary clarity to distinguish nonlinear THz-excitation pathways.

Measurements were performed on a (010) 500 μm $CdWO_4$ sample. Intense THz pulses were generated via optical rectification of (~1 mJ, ~100 fs) 1450-nm light pulses in the organic salt, nonlinear optical crystal DSTMS [34]. The THz pulses were focused to the sample with a 2-inch effective-focal-length, off-axis parabolic mirror and characterized with electro-optic sampling using a 100-μm thick (110) GaP bonded to a 1 mm thick (100) GaP slab. A collinear sensitive polarization-gating scheme [35,36] with ~100-fs 800-nm pulses was used to detect coherently excited Raman-active oscillations in $CdWO_4$ [see Fig. 1(b)]. In this detection scheme, the probe light is initially horizontally polarized and interaction with coherent Raman-active phonons can result in scattered light with rotated polarization (depolarized scattering). The induced ellipticity of the transmitted probe light is converted to changes in intensity with the combination of a $\lambda/4$ wave plate (oriented with the slow axis parallel to the initial polarization) and Wollaston polarizer, and the difference between vertical and horizontal polarizations (ΔI) is measured with balanced photodetectors. Two traces are recorded with an initial polarizer rotated to $\pm 1.4°$, and the difference between the traces is analyzed ($\Delta I_+ - \Delta I_-$) [36,37]. In the THz pump, 800-nm probe experiment, the

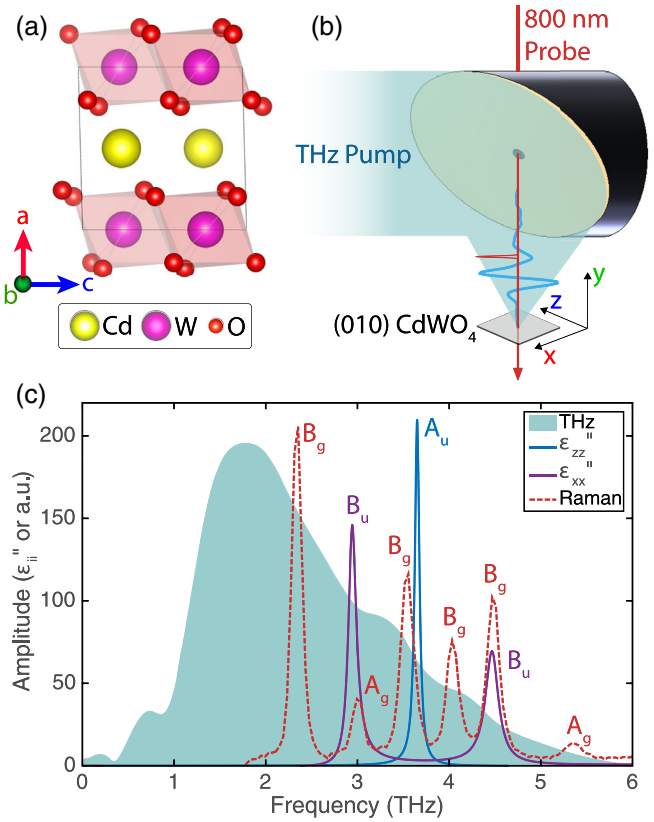

FIG. 1. (a) $CdWO_4$ crystal structure. (b) Schematic of THz pump, optical-probe measurement of $CdWO_4$. (c) Dotted red lines indicate the static Raman scattering spectrum with A_g and B_g modes labeled. The solid lines show ε'' for the A_u (blue, ε''_{zz}) and B_u (purple, ε''_{xx}) modes from Ref. [41]. The shaded region shows the THz excitation spectrum.

THz pulse can excite dipole-active modes [infrared-(IR)-active vibrations] and the 800-nm light can observe coherent Raman-active vibrations. Similar pump-probe schemes have proven useful in studying noncentrosymmetric materials like $LiNbO_3$ and Te, where vibrations that are simultaneously IR- and Raman active can be directly excited and probed [23,24,38]. But for centrosymmetric materials like $CdWO_4$ [see Fig. 1(a)], vibrational modes are either IR active or Raman active, never both. $CdWO_4$ is of the point group C_{2h}, with modes that are Raman active (A_g or B_g symmetry) or IR active (A_u or B_u symmetry). Figure 1(c) shows static Raman scattering spectra of modes with B_g and A_g symmetry (only B_g modes are observed in depolarized scattering measurements [39]), as well as absorption peaks from IR-active vibrations [41], and the experimental THz excitation spectrum. Depending on the THz polarization relative to the crystallographic axes, A_u or B_u IR-active modes within the excitation spectrum will be directly excited; however the depolarized 800-nm polarization-gating probe is only sensitive to B_g Raman-active modes.

Thus, it is surprising that when $CdWO_4$ is excited with intense THz radiation, long-lived phonon oscillations can be observed [see Fig. 2(a)], with four observed frequencies that match B_g symmetry modes seen in static Raman scattering measurements [compare peaks at 2.3, 3.5, 4.0, and 4.5 THz in Figs. 1(c) and 2(b)] [42]. We note that in comparison to measurements on noncentrosymmetric materials where modes can be directly excited and probed in such a configuration [23,24], the oscillation amplitudes observed here are very low, necessitating the more sensitive detection scheme [35,36]. Because of the low frequency of the modes, the thermal populations are fairly similar between all modes, and the differences in Raman scattering amplitudes in Fig. 1(c) are mainly due to Raman scattering cross sections. In contrast, the relative amplitudes of peaks in the THz excitation data in Fig. 2(b) are determined by a combination of the Raman-scattering cross-sections and the strength of nonlinear excitation.

In Fig. 2(c), we show how the normalized Fourier amplitudes of the four peaks from Fig. 2(b) depend on the THz polarization angle with respect to the sample. For three of the modes, we see a minimum amplitude at 0° (parallel to the crystallographic z axis) where the THz can optimally excite the A_u symmetry mode [3.5 THz, see ε''_{zz} in Fig. 1(c)] and another minimum at 90° where the B_u modes [2.9 and 4.4 THz, see ε''_{xx} in Fig. 1(c)] are most efficiently excited (parallel to the crystal x axis). The maximum in oscillation amplitude occurs at 45° (and 90° increments) when the THz polarization is right in between the optimal angles for exciting the IR-active modes. We note that one B_g mode (at 3.5 THz) has a unique angle dependence that is discussed in the Supplemental Material [39].

To better understand these results, we consider two nonlinear excitation pathways that could result in excitation of these Raman-active modes: (i) indirect excitation due to trilinear anharmonic coupling between IR- and Raman-active modes (a so-called nonlinear-phononics pathway [43–45]) and (ii) two-photon absorption (2PA) to directly excite the Raman-active modes (a nonlinear-photonics pathway) [46]. Just as higher-order correlations can easily be obscured by cascading processes [27], care must be taken to distinguish between these THz excitation routes. It is challenging to differentiate between the two, and below we show that 2D THz spectroscopy can discriminate the dominant pathway.

Because the underlying interatomic potential energy surface of $CdWO_4$ is anharmonic, vibrational modes are coupled to each other and these anharmonic couplings could be exploited to indirectly excite specific vibrational coordinates; specific IR-active modes can be resonantly excited with THz radiation to large amplitudes, which then couple to and transfer energy to other vibrations. For example, we directly excite IR-active A_u and B_u modes, which could together drive the Raman-active B_g modes that we observe. Such trilinear mode coupling has recently been posited with supporting computational work [44], yet not experimentally demonstrated. Coupling terms in the potential energy surface

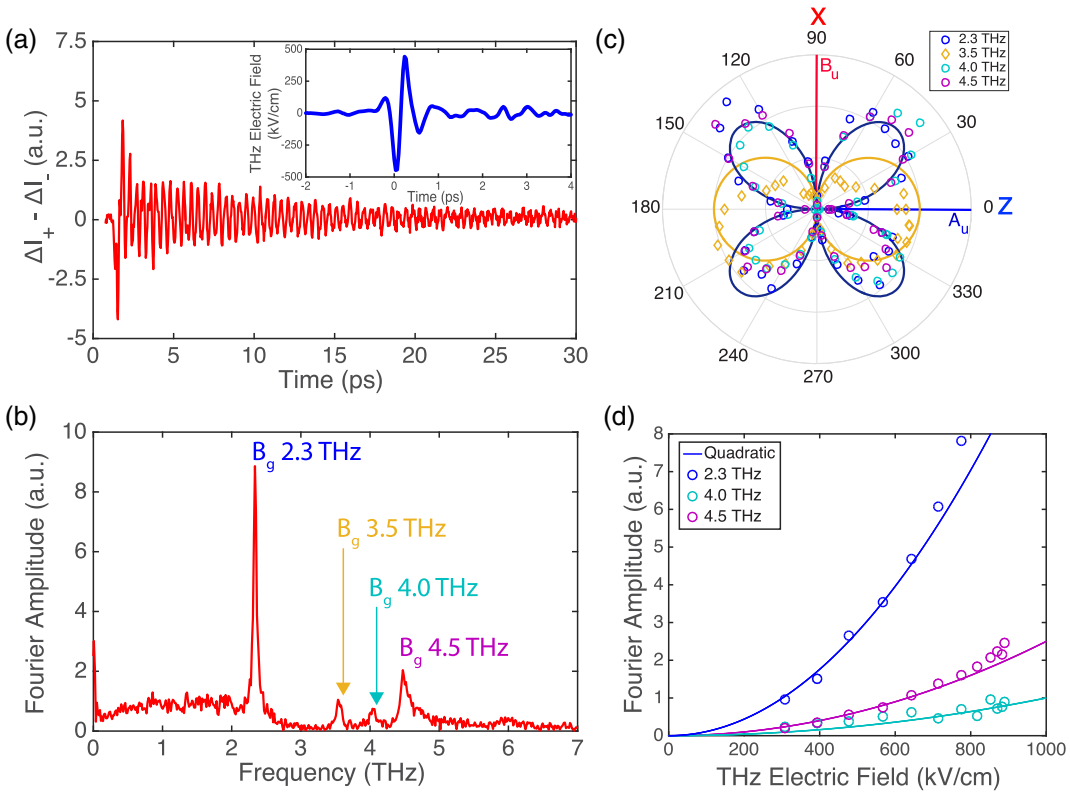

FIG. 2. (a) Observed time-domain oscillations and (b) Fourier transform showing peaks for 4 B_g vibrational modes. The inset of (a) shows the THz excitation waveform. (c) THz polarization angle dependence of (normalized) Fourier amplitudes of the four modes. The solid vertical and horizontal lines show at what angles A_u and B_u IR-active modes will be excited. The blue line shows the amplitude dependence expected from Eqs. (1) and (2). (d) The oscillation amplitudes as a function of the incident THz electric field. The solid lines show the expected quadratic dependence from Eqs. (1) and (2).

equation are only allowed if products of irreducible representations of the modes involved include the totally symmetric representation, which is A_g in $CdWO_4$ (see Supplemental Material [39]). The relevant product is $A_g \subset \langle B_g|A_uB_u\rangle$, where the symmetry elements represent the involved vibrational modes, making this type of trilinear coupling allowed in $CdWO_4$. This results in an equation of motion for Raman-active modes of

$$\ddot{Q}_R + 2\Gamma_R\dot{Q}_R + \omega_R^2 Q_R = -c_{12R}Q_{\mathrm{IR}_1}(t)Q_{\mathrm{IR}_2}(t), \quad (1)$$

where Q_R is the Raman-active mode coordinate, Γ_R is the damping rate, $\omega_R = 2\pi\nu_R$ is the angular frequency of the mode, c_{12R} is the strength of the trilinear coupling, and Q_{IR_i} are the two directly excited IR-active vibrational mode coordinates. Equation (1) is used to abbreviate the full set of coupled equations describing the excitation and energy transfer; the full equations of motion can be found in the Supplemental Material [39]. As seen with the driving term on the right-hand side of Eq. (1), if a pair of IR-active modes are simultaneously excited to large enough amplitudes, the atomic motions together can act as a driving force for Raman-active modes. For a linearly polarized THz excitation pulse, this equation predicts both maximum oscillation amplitudes at a THz polarization of 45° (when both A_u and B_u modes are excited simultaneously), as well as the quadratic amplitude dependence on incident THz electric field strength observed in Fig. 2(d) (assuming a linear Q_{IR_i} amplitude dependence on electric field strength).

The second pathway one needs to consider involves two-photon direct excitation of the Raman-active modes [46]. In 2PA an essentially identical symmetry requirement exists to allow excitation of B_g vibrational modes; one photon polarized along the crystallographic z axis behaves with A_u symmetry and while the other polarized along the x axis has B_u symmetry, resulting in the allowed excitation of B_g vibrational modes according to $\langle B_g|A_uB_u|A_g\rangle \supset A_g$ (see Supplemental Material [39]). This gives the following equation of motion

$$\begin{aligned}\ddot{Q}_R + 2\Gamma_R\dot{Q}_R + {\omega_R}^2 Q_R &= \delta_{12R}E_1(t)E_2(t) \\ &= d_{12R}\cos(\theta)\sin(\theta)E(t)^2, \quad (2)\end{aligned}$$

where δ_{12R} is the 2-THz-photon absorption cross section for the Raman-active mode, and the second equality assumes linearly polarized light at angle θ with respect to the z axis, and polarization components $E_1(t) = \cos(\theta)E(t)$ and

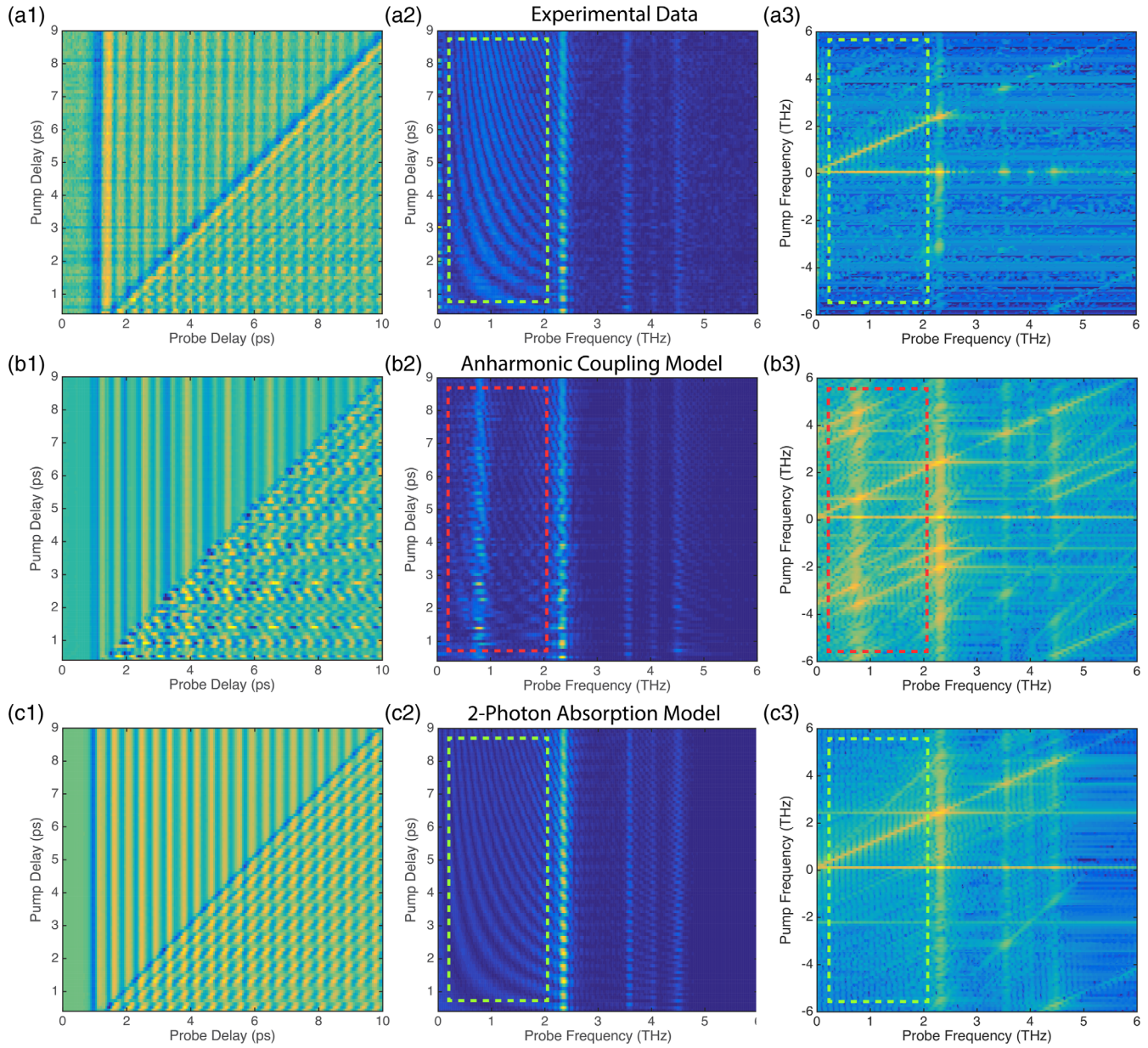

FIG. 3. 2D THz-Raman measurement of $CdWO_4$ (upper three panels) and comparison to two modeled excitation pathways (lower six panels). (a1),(b1),(c1) show the time-domain response as a function of probe delay and relative delay between two THz pump pulses. (a2),(b2),(c2) are determined by Fourier transforming along the probe-time axis. (a3),(b3),(c3) are subsequently generated by Fourier transforming along the pump-delay axis. The absolute value of the Fourier transforms is plotted. The dashed boxes highlight regions of interest showing better agreement between the experimental data and the 2PA model.

$E_2(t) = \sin(\theta)E(t)$. Both Eqs. (1) and (2) predict the maximum oscillation amplitude at 45° THz polarization, where the product of vector polarization components is at a maximum. We also note that in the case of 2PA, as above with anharmonic coupling, the oscillation amplitude should increase quadratically with the incident THz electric field as observed in Fig. 2(d). Thus, we see that both excitation routes predict the two main observations of Fig. 2: the THz-polarization dependence and the THz-electric-field dependence. These results indicate that nonlinear excitation is occurring, but are not enough to specify which excitation route is dominant. We therefore turn to 2D spectroscopy that enables us to distinguish between the excitation routes.

For 2D measurements, we generate 2 THz pulses with a variable delay, and we observe the sample response with the same 800-nm probing scheme. This represents what has been termed a 2D THz-THz-Raman (TTR) measurement scheme [32,33,47]. The false-color plot in Fig. 3(a1) shows the oscillatory signal as a function of the relative 800-nm probe delay on the x axis and relative delay between the

two THz pump pulses along the y axis. The very top line of Fig. 3(a1), when the timing between THz pump pulses is as large as the probe window (10 ps), would essentially reproduce the data shown in Fig. 2(a). We can clearly see that the oscillatory response [after the second pump pulse–the diagonal feature in Fig. 3(a1)] is strongly influenced by the relative delay of the two pump pulses. This is even more clear in Fig. 3(a2), where we have taken the Fourier transform along the probe time axis; the magnitude of the Fourier peaks from the 4 oscillations vary strongly with pump delay, each with unique spacing. By varying the pump delay, we can control the energy flow to shut off certain frequencies while exciting others in a clear demonstration of coherent control. Next, we take the Fourier transform along the pump-delay axis to create Fig. 3(a3) and show how the sample frequency response varies with excitation frequency.

To analyze the sample response, and compare to our proposed excitation routes, we use Eqs. (1) and (2) to model the 2D signal for both cases. Figure 3, panels (b1), (b2), (b3) show the modeled anharmonic coupling response [Eq. (1)] and panels (c1), (c2), (c3) show the modeled 2PA response [Eq. (2)]. First, we see that both models reproduce well the spectral amplitudes of the vibrations when comparing Figs. 3(b2) and 3(c2) to Fig. 3(a2). Some differences are noticed when comparing the modeled time-domain responses to each other and the data [3(a1), 3(b1), 3(c1)], but when we compare the two varieties of frequency domain data [3(a2), 3(b2), 3(c2) or 3(a3), 3(b3), 3(c3)], important differences become more apparent, most notably in the region outlined by dashed rectangles. The experimental data lack a prominent feature just below 1 THz that is present in the anharmonic coupling model [see Figs. 3 (b2) and 3(b3)] that, according to the model, would result from strong driving of atomic motion at the difference frequency of two excited IR-active vibrations. The 2PA model lacks this feature and overall has very good agreement with experiment. Therefore, we conclude that the two-photon excitation pathways dominate the observed results.

Here we have shown that intense THz pulses can nonlinearly excite a set of Raman-active vibrational modes. We considered anharmonic phonon coupling and 2PA excitation routes and showed that single-pulse excitation measurements were not enough to unambiguously distinguish the dominant excitation pathway. These results have important general implications for the rising field of nonlinear phononics [23,43–45,48,49]. For example, an anharmonic coupling mechanism was used to explain the single-pulse excitation results in Ref. [43] that introduced the concept of nonlinear phononics, but a multiphoton (difference frequency) pathway could possibly also explain the observations. 2D THz-Raman spectroscopic analysis allowed us to distinguish between photonic and phononic excitation pathways and determine that 2PA is the dominant excitation pathway in $CdWO_4$. As more systems are studied with high-field THz radiation to explore fundamental material properties and cutting-edge device development, multidimensional measurements will be needed to elucidate energy transfer pathways.

The authors acknowledge funding from the Department of Chemistry and Biochemistry and the College of Physical and Mathematical Sciences at Brigham Young University. They would also like to thank Professor Eric Sevy for discussions regarding absorption selection rules.

*jjohnson@chem.byu.edu

[1] J. B. Baxter and G. W. Guglietta, Terahertz spectroscopy, Anal. Chem. **83**, 4342 (2011).
[2] W. L. Chan, J. Deibel, and D. M. Mittleman, Imaging with terahertz radiation, Rep. Prog. Phys. **70**, 1325 (2007).
[3] W. Zouaghi, M. D. Thomson, K. Rabia, R. Hahn, V. Blank, and H. G. Roskos, Broadband terahertz spectroscopy: Principles, fundamental research and potential for industrial applications, Eur. J. Phys. **34**, S179 (2013).
[4] A. A. Gowen, C. O'Sullivan, and C. P. O'Donnell, Terahertz time domain spectroscopy and imaging: Emerging techniques for food process monitoring and quality control, Trends Food Sci. Technol. **25**, 40 (2012).
[5] K. Shiraga, Y. Ogawa, T. Suzuki, N. Kondo, A. Irisawa, and M. Imamura, Determination of the complex dielectric constant of an epithelial cell monolayer in the terahertz region, Appl. Phys. Lett. **102**, 053702 (2013).
[6] I. F. Akyildiz, J. M. Jornet, and C. Han, Terahertz band: Next frontier for wireless communications, Phys. Chem. Comm. **12**, 16 (2014).
[7] F. D. J. Brunner, O. P. Kwon, S.-J. Kwon, M. Jazbinšek, A. Schneider, and P. Günter, A hydrogen-bonded organic nonlinear optical crystal for high-efficiency terahertz generation and detection, Opt. Express **16**, 16496 (2008).
[8] H. Hirori, A. Doi, F. Blanchard, and K. Tanaka, Single-cycle terahertz pulses with amplitudes exceeding 1 MV/cm generated by optical rectification in LiNbO3, Appl. Phys. Lett. **98**, 091106 (2011).
[9] C. H. Matthias and F. József András, Intense ultrashort terahertz pulses: Generation and applications, J. Phys. D **44**, 083001 (2011).
[10] C. Ruchert, C. Vicario, and C. P. Hauri, Scaling submillimeter single-cycle transients toward megavolts per centimeter field strength via optical rectification in the organic crystal OH1, Opt. Lett. **37**, 899 (2012).
[11] C. Ruchert, C. Vicario, and C. P. Hauri, Spatiotemporal Focusing Dynamics of Intense Supercontinuum THz Pulses, Phys. Rev. Lett. **110**, 123902 (2013).
[12] C. Vicario, M. Jazbinsek, A. V. Ovchinnikov, O. V. Chefonov, S. I. Ashitkov, M. B. Agranat, and C. P. Hauri, High efficiency THz generation in DSTMS, DAST and OH1 pumped by Cr: forsterite laser, Opt. Express **23**, 4573 (2015).
[13] K.-L. Yeh, M. C. Hoffmann, J. Hebling, and K. A. Nelson, Generation of 10 μJ ultrashort terahertz pulses by optical rectification, Appl. Phys. Lett. **90**, 171121 (2007).
[14] M. Clerici, M. Peccianti, B. E. Schmidt, L. Caspani, M. Shalaby, M. Giguère, A. Lotti, A. Couairon, F. Légaré,

T. Ozaki, D. Faccio, and R. Morandotti, Wavelength Scaling of Terahertz Generation by Gas Ionization, Phys. Rev. Lett. **110**, 253901 (2013).

[15] K. Y. Kim, J. H. Glownia, A. J. Taylor, and G. Rodriguez, High-power broadband terahertz generation via two-color photoionization in gases, IEEE J. Quantum Electron. **48**, 797 (2012).

[16] H. Y. Hwang, S. Fleischer, N. C. Brandt, B. G. Perkins, M. Liu, K. Fan, A. Sternbach, X. Zhang, R. D. Averitt, and K. A. Nelson, A review of non-linear terahertz spectroscopy with ultrashort tabletop-laser pulses, J. Mod. Opt. **62**, 1447 (2015).

[17] T. Kampfrath, K. Tanaka, and K. A. Nelson, Resonant and nonresonant control over matter and light by intense terahertz transients, Nat. Photonics **7**, 680 (2013).

[18] M. M. Jadidi, J. C. König-Otto, S. Winnerl, A. B. Sushkov, H. D. Drew, T. E. Murphy, and M. Mittendorff, Nonlinear terahertz absorption of graphene plasmons, Nano Lett. **16**, 2734 (2016).

[19] Y. Minami, K. Araki, T. D. Dao, T. Nagao, M. Kitajima, J. Takeda, and I. Katayama, Terahertz-induced acceleration of massive Dirac electrons in semimetal bismuth, Sci. Rep. **5**, 15870 (2015).

[20] K. Fan, H. Y. Hwang, M. Liu, A. C. Strikwerda, A. Sternbach, J. Zhang, X. Zhao, X. Zhang, K. A. Nelson, and R. D. Averitt, Nonlinear Terahertz Metamaterials via Field-Enhanced Carrier Dynamics in GaAs, Phys. Rev. Lett. **110**, 217404 (2013).

[21] C. Lange, T. Maag, M. Hohenleutner, S. Baierl, O. Schubert, E. R. J. Edwards, D. Bougeard, G. Woltersdorf, and R. Huber, Extremely Nonperturbative Nonlinearities in GaAs Driven by Atomically Strong Terahertz Fields in Gold Metamaterials, Phys. Rev. Lett. **113**, 227401 (2014).

[22] M. Liu, H. Y. Hwang, H. Tao, A. C. Strikwerda, K. Fan, G. R. Keiser, A. J. Sternbach, K. G. West, S. Kittiwatanakul, J. Lu, S. A. Wolf, F. G. Omenetto, X. Zhang, K. A. Nelson, and R. D. Averitt, Terahertz-field-induced insulator-to-metal transition in vanadium dioxide metamaterial, Nature (London) **487**, 345 (2012).

[23] B. S. Dastrup, J. R. Hall, and J. A. Johnson, Experimental determination of the interatomic potential in LiNbO3 via ultrafast lattice control, Appl. Phys. Lett. **110**, 162901 (2017).

[24] A. von Hoegen, R. Mankowsky, M. Fechner, M. Först, and A. Cavalleri, Probing the interatomic potential of solids with strong-field nonlinear phononics, Nature (London) **555**, 79 (2018).

[25] T. Kubacka *et al.*, Large-amplitude spin dynamics driven by a THz pulse in resonance with an electromagnon, Science **343**, 1333 (2014).

[26] K. S. Schmidt-Rohr and H. W. Spiess, *Multidimensional Solide-State NMR and Polymers* (Academic Press, New York, 1994).

[27] S. Mukamel, *Principles of Nonlinear Optics and Spectroscopy* (Oxford University Press, New York, 1995).

[28] W. Kuehn, K. Reimann, M. Woerner, T. Elsaesser, and R. Hey, Two-dimensional terahertz correlation spectra of electronic excitations in semiconductor quantum wells, J. Phys. Chem. B **115**, 5448 (2011).

[29] M. Woerner, W. Kuehn, P. Bowlan, K. Reimann, and T. Elsaesser, Ultrafast two-dimensional terahertz spectroscopy of elementary excitations in solids, New J. Phys. **15**, 025039 (2013).

[30] J. Lu, X. Li, H. Y. Hwang, B. K. Ofori-Okai, T. Kurihara, T. Suemoto, and K. A. Nelson, Coherent Two-Dimensional Terahertz Magnetic Resonance Spectroscopy of Collective Spin Waves, Phys. Rev. Lett. **118**, 207204 (2017).

[31] J. Lu, Y. Zhang, H. Y. Hwang, B. K. Ofori-Okai, S. Fleischer, and K. A. Nelson, Nonlinear two-dimensional terahertz photon echo and rotational spectroscopy in the gas phase, Proc. Natl. Acad. Sci. U.S.A. **113**, 11800 (2016).

[32] I. A. Finneran, R. Welsch, M. A. Allodi, T. F. Miller, and G. A. Blake, Coherent two-dimensional terahertz-terahertz-Raman spectroscopy, Proc. Natl. Acad. Sci. U.S.A. **113**, 6857 (2016).

[33] I. A. Finneran, R. Welsch, M. A. Allodi, T. F. Miller, and G. A. Blake, 2D THz-THz-Raman photon-echo spectroscopy of molecular vibrations in liquid bromoform, J. Phys. Chem. Lett. **8**, 4640 (2017).

[34] Z. Yang, L. Mutter, M. Stillhart, B. Ruiz, S. Aravazhi, M. Jazbinsek, A. Schneider, V. Gramlich, and P. Günter, Large-size bulk and thin-film stilbazolium-salt single crystals for nonlinear optics and THz generation, Adv. Funct. Mater. **17**, 2018 (2007).

[35] F. D. J. Brunner, J. A. Johnson, S. Grübel, A. Ferrer, S. L. Johnson, and T. Feurer, Distortion-free enhancement of terahertz signals measured by electro-optic sampling. I. Theory, J. Opt. Soc. Am. B **31**, 904 (2014).

[36] J. A. Johnson, F. D. J. Brunner, S. Grübel, A. Ferrer, S. L. Johnson, and T. Feurer, Distortion-free enhancement of terahertz signals measured by electro-optic sampling. II. Experiment, J. Opt. Soc. Am. B **31**, 1035 (2014).

[37] C. A. Werley, S. M. Teo, and K. A. Nelson, Pulsed laser noise analysis and pump-probe signal detection with a data acquisition card, Rev. Sci. Instrum. **82**, 123108 (2011).

[38] T. Huber, M. Ranke, A. Ferrer, L. Huber, and S. L. Johnson, Coherent phonon spectroscopy of non-fully symmetric modes using resonant terahertz excitation, Appl. Phys. Lett. **107**, 091107 (2015).

[39] See Supplemental Material at http://link.aps.org/supplemental/10.1103/PhysRevLett.122.073901 for a more detailed and complete treatment of modeling the sample response for possible excitation pathways, which includes Ref. [40].

[40] E. Kroumova, M. I. Aroyo, J. M. Perez-Mato, A. Kirov, C. Capillas, S. Ivantchev, and H. Wondratschek, Bilbao crystallographic server: Useful databases and tools for phase-transition studies, Phase Transitions **76**, 155 (2003).

[41] A. Mock, R. Korlacki, S. Knight, and M. Schubert, Anisotropy, phonon modes, and lattice anharmonicity from dielectric function tensor analysis of monoclinic cadmium tungstate, Phys. Rev. B **95**, 165202 (2017).

[42] R. Lacomba-Perales, D. Errandonea, D. Martinez-Garcia, P. Rodríguez-Hernández, S. Radescu, A. Mujica, A. Muñoz, J. C. Chervin, and A. Polian, Phase transitions in wolframite-type $CdWO_4$ at high pressure studied by Raman spectroscopy and density-functional theory, Phys. Rev. B **79**, 094105 (2009).

[43] M. Forst, C. Manzoni, S. Kaiser, Y. Tomioka, Y. Tokura, R. Merlin, and A. Cavalleri, Nonlinear phononics as an ultrafast route to lattice control, Nat. Phys. **7**, 854 (2011).

[44] D. M. Juraschek, M. Fechner, and N. A. Spaldin, Ultrafast Structure Switching Through Nonlinear Phononics, Phys. Rev. Lett. **118**, 054101 (2017).

[45] A. Subedi, A. Cavalleri, and A. Georges, Theory of nonlinear phononics for coherent light control of solids, Phys. Rev. B **89**, 220301 (2014).

[46] S. Maehrlein, A. Paarmann, M. Wolf, and T. Kampfrath, Terahertz Sum-Frequency Excitation of a Raman-Active Phonon, Phys. Rev. Lett. **119**, 127402 (2017).

[47] T. Ikeda, H. Ito, and Y. Tanimura, Analysis of 2D THz-Raman spectroscopy using a non-Markovian Brownian oscillator model with nonlinear system-bath interactions, J. Chem. Phys. **142**, 212421 (2015).

[48] R. Mankowsky, A. von Hoegen, M. Först, and A. Cavalleri, Ultrafast Reversal of the Ferroelectric Polarization, Phys. Rev. Lett. **118**, 197601 (2017).

[49] A. Subedi, Proposal for ultrafast switching of ferroelectrics using midinfrared pulses, Phys. Rev. B **92**, 214303 (2015).